Phase Field Modeling of Coupled Phase Separation and Diffusion Induced Stress in Lithium Iron Phosphate Particles Reconstructed from Synchrotron Nano X-ray Tomography

Linmin Wu[1], Xianghui Xiao[2,3], Jing Zhang[1,*]

[1]Department of Mechanical and Energy Engineering, Indiana University-Purdue University Indianapolis, Indianapolis, IN 46202, USA

[2]Advanced Photon Source, Argonne National Laboratory, 9700 Cass Ave, Lemont, IL 60439

[3]National Synchrotron Light Source II (NSLS-II), Brookhaven National Laboratory, 98 Rochester St, Upton, NY 11973

*Corresponding author: jz29@iupui.edu

Abstract

In this study, the phase separation phenomenon and diffusion induced stresses in lithium iron phosphate ($LiFePO_4$) particles under potentiostatic discharging process have been simulated using the phase field method. The realistic particles reconstructed from synchrotron nano X-ray tomography, along with idealized spherical and ellipsoid shaped particles were studied. The results show stress and diffusion process in particles are strongly influenced by particle shapes, especially at the initial lithiation stage. Stresses in the realistic particles are higher than idealized spherical ones by at least 30%. The diffusion induced hydrostatic stress has a strong relationship with lithium ion concentration. The hydrostatic stresses and first principal stresses tend to shift from lower values to higher values as the particle takes in more lithium ions. Additionally, the diffusion induced stresses are related to the maximum concentration difference in the particle. High concentration difference will cause high stresses. In ellipsoid particles, the stress levels

This is the author's manuscript of the article published in final edited form as:

Wu, L., Andrade, V. D., Xiao, X., & Zhang, J. (2019). Phase Field Modeling of Coupled Phase Separation and Diffusion-Induced Stress in Lithium Iron Phosphate Particles Reconstructed From Synchrotron Nano X-ray Tomography. Journal of Electrochemical Energy Conversion and Storage, 16(4), 041006. https://doi.org/10.1115/1.4043155

increase with the aspect ratios. The model provides a design tool to optimize the performance of cathode materials with phase separation phenomena.

Keywords: synchrotron X-ray tomography; $LiFePO_4$; phase separation; stress; phase field model

1. Introduction

Lithium ion rechargeable batteries (LIBs) are considered as good candidates for portable electronics and electric vehicles applications, due to their high energy and power density [1-3]. Among all electrode materials, lithium iron phosphate ($LiFePO_4$) is one of the most promising cathode materials due to its low cost, low toxicity and excellent rate performance [4, 5]. $LiFePO_4$ is also known for its two-phase structure [6-8]. Many technological improvements have been made to increase the performance of $LiFePO_4$, including enhancing its electronic and ionic conductivity [9-11] and increasing surface chemical stability [12-15]. One of the challenges of $LiFePO_4$ is to understand its two-phase structure and enhance the mechanical stability. Diffusion induced stresses [16-18] done by our group, and phase separation [19-21] during the operations of batteries have shown to cause fracture and mechanical failure in electrodes and cells. Hence, it is important to understand the coupled phase change and diffusion induced stress generation in $LiFePO_4$.

Many studies have been done to study the stress generation to prevent the mechanical failures of LIBs [18, 22-26]. Zhang *et al.* [24, 25] studied the stress generation in $LiMn_2O_4$ under galvanostatic and potentiodynamic conditions using ellipsoid shaped particle model. Cheng and Verbrugge [23, 27, 28] investigated the diffusion induced stresses in spherical and nanowire electrodes. Zhao *et al.* [22, 29] and Woodford *et al.*[30] simulated the stress levels and evaluated the failure criterion for battery particles. However, many of these studies employed single spherical particle model, and the diffusion kinetics and electrochemical processes were simplified greatly. There were some attempts to simulate the stress generation of realistic microstructures in LIBs. Zhang *et al.* [31] studied the diffusion induced stresses of realistic geometry of $LiMn_2O_4$ particles reconstructed by atomic force microscopy. Wu *et al.* [32]

investigated the mechanical behavior of $LiMn_2O_4$ cathode reconstructed by 2D SEM images under discharge conditions. The phase separation was not considered in the study.

Stresses caused by phase separation inside the electrode materials, such as $LiFePO_4$, can be detrimental to electrode particles. Phase separation can cause volume changes to the structure, leading to structure instability. ChiuHuang and Huang [33] investigated the stress evolution on the phase boundary of $LiFePO_4$ particles. Renganathan *et al.* [20] simulated the stress inside the porous electrode by taking advantage of the P2D model including moving phase boundary. However, they used moving boundary method to track the phase boundary explicitly. This method can only be applied to simple geometry and not robust in complex shaped particles due to numerical convergence issue. Phase field method is a promising technique [34] to describe the microstructural evolution. The method is applied to model multiphase microstructure evolution without tracking the phase boundary explicitly [35, 36] and is robust in complex geometries [37, 38]. Recently, Lei *et al.* [39] studied large elasto-plastic deformation in lithiated silicon electrode by phase field method. Welland *et al.* [40] applied phase field method to investigate phase evolution in $LiFePO_4$ particles.

Given the discussions above, there is no previous work on studying the coupled diffusion, phase separation and stress effects in realistic lithium iron phosphate particles reconstructed from synchrotron nano X-ray tomography. In this paper, the phase field method will be employed to simulate the phase evolution and stress generation of $LiFePO_4$ in realistic shaped particles, along with ideal spherical and ellipsoid shapes for comparison. The model will provide a design tool to optimize the performance of battery materials with phase separation phenomena, such as $LiFePO_4$.

The paper is organized as follows: In section 2, the method of synchrotron nano-CT imaging processing and microstructure reconstruction of $LiFePO_4$ particles are given. In section 3, a set of mathematical formulations describing the diffusion and the stresses in $LiFePO_4$ particles are listed. In section 4, the phase separation induced lithium ion concentration distributions and diffusion induced stress levels in spherical, ellipsoid and realistic particles are discussed and analyzed. Conclusions are given in section 5.

2. Reconstruction of $LiFePO_4$ particle microstructures

The microstructures of $LiFePO_4$ particles used for the model were obtained by synchrotron X-ray tomography at beamlines 32-ID-C and 2-BM at the Advanced Photon Source, Argonne National Laboratory. Synchrotron X-ray can offer high brightness multi-level views with less artifacts and high resolutions, which is ideal for microstructure reconstruction. The $LiFePO_4$ cathode used in the experiment was from a commercial LG HE4 18650 cell. The fresh $LiFePO_4$ 18650 cell was disassembled in argon filled glove box, and the cathode materials were carefully scratched off. A set of gray-scale images were obtained with a voxel size of 30 nm after synchrotron X-ray tomography. The carbon and binder phases were neglected in this study, because it is hard to distinguish them from the background. In order to reduce the computational cost, an edge preserving smoothing filter and small islands removal filters were applied followed by greyscale threshold segmentation. After image processing and reconstruction, two realistic $LiFePO_4$ particles were extracted, as shown in Figure 1. The two extracted particles have equivalent radius of 0.402 μm and 0.548 μm, respetively. The equivalent radius R is defined as $R=(3V/4\pi)^{1/3}$, where V is volume of the particle. The meshed particles were imported into Comsol Multiphysics for further simulation.

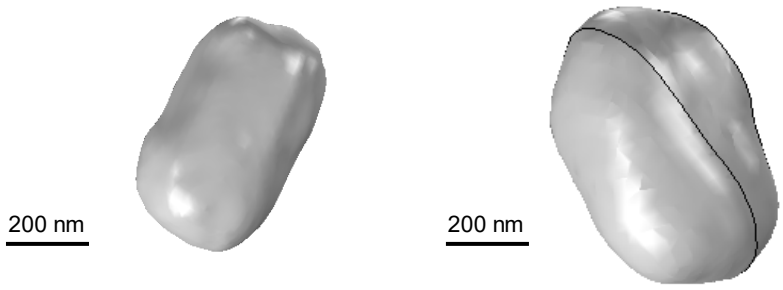

(a) (b)

Fig. 1. $LiFePO_4$ particles reconstructed from nano X-ray tomography. (a) 0.402 μm equivalent radius; (b) 0.548 μm equivalent radius.

3. Model description

The mathematical model consists of diffusion sub-model and mechanics sub-model. The diffusion model describes the species transports in $LiFePO_4$ particles for phase separation analysis. The mechanics model computes the diffusion induced stresses in particles during lithium ion intercalation process.

3.1 Mechanics sub-model

The mechanics model computes the stresses and particle deformations in $LiFePO_4$ particles. The total strain ε_{ij} contains the mechanical strain ε_{ij}^{me} and the diffusion induced strain. The diffusion induced strain is formulated by the thermal analogy [20, 23]. The constitutive equation describing the stress and strain before phase transition is given by:

$$\varepsilon_{ij} = \varepsilon_{ij}{}^{me} + \varepsilon_{ij}{}^{dis} = \frac{1}{E}\left[(1+\upsilon)\sigma_{ij} - \upsilon\sigma_{kk}\delta_{ij}\right] + \frac{\hat{c}\Omega}{3}\delta_{ij} \quad (1)$$

where E is Young's modulus; υ is Poisson's ratio; σ_{ij} is stress tensor; $\hat{c}$ is the concentration difference of lithium ions from the original value; Ω is the partial molar volume.

The stress components obey mechanical equilibrium:

$$\sigma_{ij,j} = 0 \tag{2}$$

3.2 Diffusion sub-model

In order to describe the phase separation phenomenon in $LiFePO_4$ particles, a Cahn-Hilliard type free energy functional is adopted [41, 42]. The total free energy density is comprised of three parts:

$$\Psi_{total} = \Psi_{chemical} + \Psi_{interface} + \Psi_{elastic} \tag{3}$$

where $\Psi_{chemical}$, $\Psi_{interface}$ and $\Psi_{elastic}$ are bulk chemical free energy density, interface free energy density and elastic strain energy density, respectively.

The bulk chemical free energy density depends on local concentration and is expressed by regular solution model [41, 43]:

$$\Psi_{chemical} = RTc_{max}[c\ lnc + (1-c)\ ln(1-c)] + RTc_{max}\chi c\ (1-c) \tag{4}$$

where R is gas constant; T is temperature; χ is a parameter used to represent phase separation.

The interface free energy density is a function of the concentration gradient and represents the energy penalty for the phase interface:

$$\Psi_{interface} = \frac{1}{2} c_{max} k |\nabla c|^2 \tag{5}$$

where k is interface parameter.

The strain energy density is formulated as:

$$\Psi_{elastic} = \frac{1}{2}\varepsilon_{ij}\sigma_{ij} \tag{6}$$

The diffusion process in $LiFePO_4$ particles is given by:

$$\frac{\partial c}{\partial t} = -\nabla \cdot (-M\nabla\mu) \tag{7}$$

where M is the degenerated mobility and is represented by $M = Dc(1-c)$; μ is the chemical potential, which is the variational derivative of the total free energy density with respect to the local concentration, $\mu = \partial\Psi_{total}/\partial c$. If the contributions of the interface and elastic energy are neglected, the chemical potential $\mu = lnc - ln(1-c) + \chi(1-2c)$.

3.3 Boundary conditions, material properties and nondimensionalization

For the diffusion sub-model, on the particle surface, the reaction rate is described by Butler-Volmer relationship [42, 44]:

$$j_s = c_s \frac{a_+^{1-\beta} a^{\beta}}{\tau_0 \gamma}\left[exp\left(-\beta\frac{F\eta}{RT}\right) - exp\left((1-\beta)\frac{F\eta}{RT}\right)\right] \tag{8}$$

where c_s is the concentration of intercalation sites on the particle surface. τ_0 is the mean time for a single reaction step, which is set to 1 [44]. γ is the chemical activity coefficient of the active state [45], which is $(1 - c/c_{max})^{-1}$. β is the symmetric factor for a forward and backward reaction, which is 0.5. The parameters a_+, a and a_- are the activity of lithium ion in the electrolyte, lithium in the host material and electrons, respectively. Due to the fast diffusion of lithium ion in the electrolyte and fast migration of electrons, a_+ and a_- are set to 1. η is the surface overpotential, which is expressed as [35],

$$\eta = \frac{1}{F}[\mu_{Li} - \mu_{Li^+} - -\mu_{e^-}] = \frac{1}{F}\mu + \varphi_e - \varphi = \frac{1}{F}\mu + \Delta\varphi \tag{9}$$

where φ_e is the electrostatic potential of the electrode and φ denotes that of the electrolyte. $\Delta\varphi$ is the voltage drop across the electrode-electrolyte interface. In this study, potentiostatic discharging condition is applied on particle surface. Given the potential difference, the particle will take in lithium ions, evolve from lithium-poor phase towards lithium-rich phase and reaches equilibrium. With the galvanostatic charging condition, however, the local lithium ion concentration may exceed the maximum concentration, and caution should be applied to avoid system instability.

For the mechanics sub-model, traction-free boundary condition is applied on the particle surface and rigid body motion is suppressed.

According to Ref. [46], the two phase coexistence region of Li_XFePO_4 is in the range of $0.032 \leq X \leq 0.968$. The phase separation parameter χ is fitted to be 3.56 to produce a two phase region $0.035 \leq X \leq 0.965$. The partial molar volume, Young's modulus and Poisson's ratio are calculated from Ref. [47]. The material properties used in the model are listed in Table 1.

In order to achieve good convergence, the physical quantities mentioned above need to be nondimentionalized. The normalized Li concentration, space and time coordinates are given by:

$$\tilde{c} = \frac{c}{c_{max}}, \tilde{x} = \frac{x}{L}, \tilde{t} = \frac{D}{L^2}t \tag{10}$$

where L is the characteristic length. Quantities such as chemical potential, stress, Young's modulus and overpotential are normalized as:

$$\tilde{\mu} = \frac{\mu}{RT}, \tilde{\sigma} = \frac{\sigma}{RTc_{max}}, \tilde{E} = \frac{E}{RTc_{max}}, \tilde{\eta} = \frac{F\eta}{RT} \tag{11}$$

Table 1: Material properties used in the model with reference source

Initial normalized concentration $\widetilde{c_0}$	0.03
Maximum concentration c_{max}	21190 mol m-3 [48]
Diffusivity D	7.0×10^{-15} m^2 s-1 [49]
Young's modulus E	108.1 GPa [47]
Poisson's ratio υ	0.23 [47]
Partial molar volume Ω	2.307×10^{-6} m^3 mol-1 [47]
Interface parameter k	1×10^{-10} Jm^2 mol-1 [43]
Phase separarion parameter χ	3.56
Voltage drop across interface $\Delta\varphi$	-25 mV
Characteritic length L	1 μm
Temperature T	296 K

4. Results and discussion

The mathematical model described in section 3 was implemented in Comsol Multiphysics PDE module. The simulation time step was set to 0.001 s. The spherical particles, ellipsoid particles and realistic-shaped particles of $LiFePO_4$ were simulated, independently. The $LiFePO_4$ particles were potentiostaticaly discharged from initial lithium-poor phase to equilibrium lithium-rich phase.

To study the diffusion process in phase separating electrodes, the lithium concentration and hydrostatic stress profiles in the spherical, ellipsoid and realistic particles are shown in Fig.

2. Here, the state of charge (SOC) is defined as the ratio of the average local lithium ion concentration to the stoichiometric lithium ion concentration in $LiFePO_4$ particles. For the ellipsoid particle, the lengths of three semiaxes a, b, and c satisfy a = b, and the aspect ratio is defined as c/a.

For all these three cases, core-shell structures are obtained, which is in agreement with the experimental observation [50]. During discharge, the Li-rich phase initiates from the outer surface and propagates to the inner region subsequently. The hydrostatic stresses in Fig. 2 (d), (e) and (f) are relevant to corresponding lithium ion concentration profiles in (a), (b) and (c). It can also be observed that the compressive stresses build up in shell regions and tensile stresses accumulate in the core areas, though the particle surfaces are without any mechanical constraints.

The diffusion process in particles are strongly influenced by particle shapes, especially at the initial lithiation stage. For example, when SOC is 0.25, the concentration distributions are very different. For ellipsoid particles, the Li-rich phase initiates around the equator tip first, and then occurs around the semi-minor axis, which is unlike the homogeneous Li-rich phase propagation from surface to center in spherical particle. For realistic particles with rough surfaces, the Li-rich phase occurs at the convex area first, and then propagates to the rest of the particle. The inhomogeneous concentration distributions will also affect the stress distribution, as shown in Fig. 2 (e) and (f). The ellipsoid particle and realistic particle tend to have higher stresses than the spherical one. Thus, it is very important to understand the geometry effect on stress.

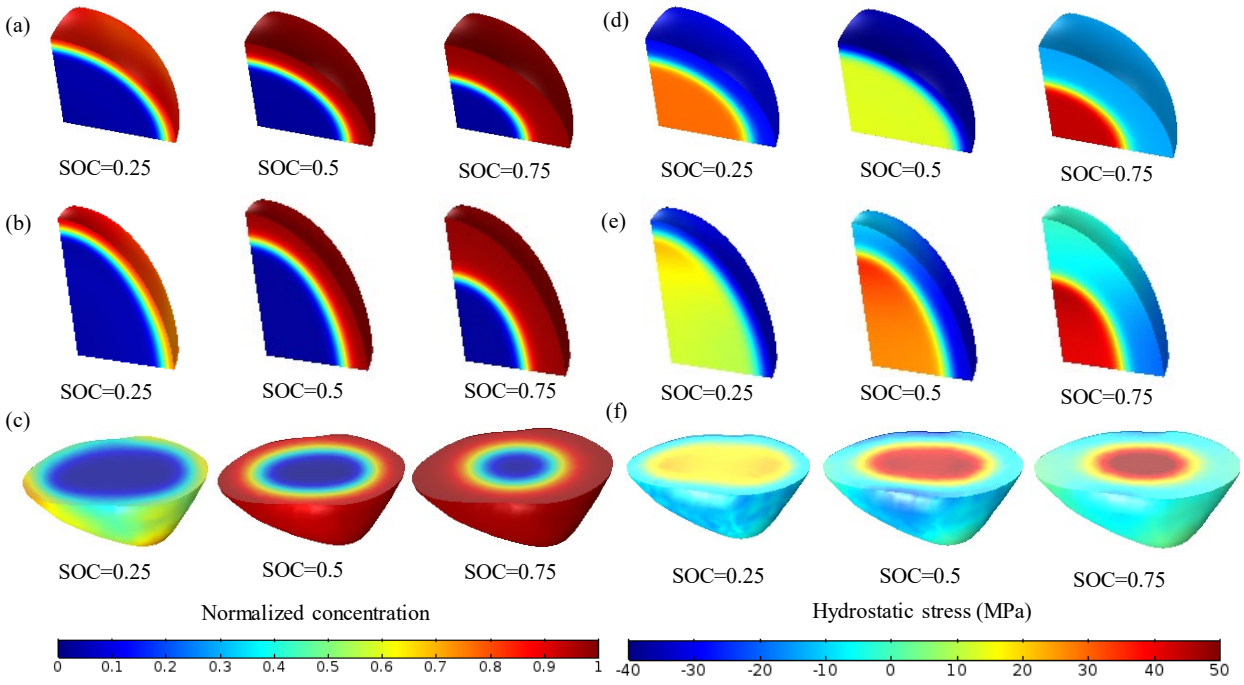

Fig. 2. Lithium ion concentration and hydrostatic stresses for different SOC. (a) and (d) are concentration distribution and hydrostatic stresses for spherical particle with 1 μm radius; (b) and (e) are those for ellipsoid particle with 1 μm equivalent radius and 1.414 aspect ratio; (c) and (f) are those for realistic particle with 0.548 μm equivalent radius.

To better understand the diffusion process and stress generation in spherical particles, the concentration distributions and stresses are plotted in Fig. 3. During the discharging, the lithium ions flow from the outer suface into the inner regions. As shown in Fig. 3 (a), the phase separation phenomenon can be cleary seen, and the phase boundary has a smoothly transitioned lithium ion concentration. The Li-rich phase has a normalized concentration about 0.965, while the Li-poor phase is about 0.035. The corresponding hydrostatic stresses change smoothly at the phase boundary regions, as shown in Fig. 3 (b). The hydrostatic stresses tend to shift from lower values to higher values as the particle takes in more lithium ions. In order to evaulate the failure

of the particle, the first principal stress was introduced. In Fig. 3 (c), the development of the first principal stress has a similar trend as the hydrostatic stress, shifting from lower values to higher values. The maximum first principal stresses always occur at the center of the spherical particle. The first principal stresses have values of 0 at the out surface due to lack of mechanical constraints on outer surface.

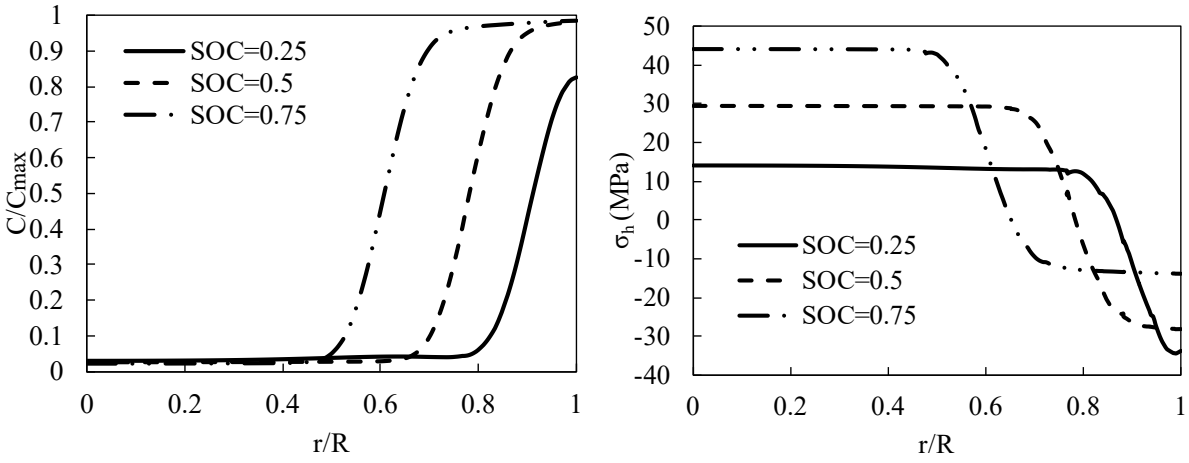

(a) (b)

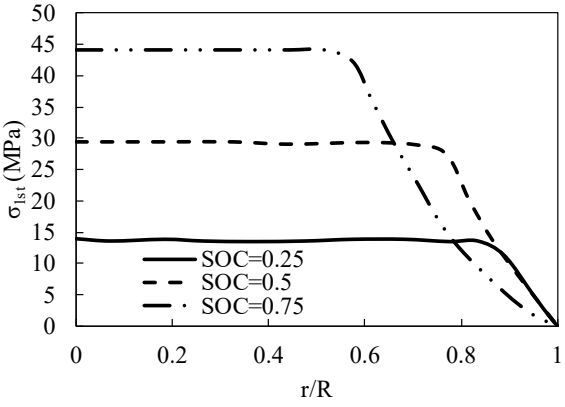

(c)

Fig. 3. Concentration and stresses along radial axis for spherical $LiFePO_4$ particle with 1 μm radius.(a) Concentration distributions; (b) Hydrostatic stresses; (c) First principal stresses.

In order to study the geometry effect on diffusion induced stresses, the maximum principal stress in the ellipsoid particles was studied. Here, to better compare the stress levels in the ellipsoid particles with the spherical one, the volumes of the particles were kept constant while the aspect ratios were varied. It is found that the history of the maximum first principal stress has a relationship with the maximum concentration difference in the particles. Maximum concentration difference is defined as max lithium concentration difference in the particle. As seen in Fig. 4, with the discharging, the maximum concentration difference will increase. In the meantime, the stress levels also increase. After the systems reach equilibirum, corresponding to the drop of the concentration difference, the stress levels will reduce due to less concentration gradient. From Fig. 4 (a), particles with higher aspect ratios have a higher concentration difference, especially at the initial discharging. For example, when SOC is around 0.15, the maximum concentration difference for particle with aspect ratio 2 is about 0.86, which it almost doubles the values of the spherical particle. In the meantime, the corresponding first principal stress in aspect ratio 2 particle is around 26 MPa, which is about 2.4 times the stress in the sperical one.

It can also be concluded that particles with larger aspect ratios always have higher stress levels than those lower aspect ratios, as shown in Fig. 4 (b). The maximum first principal stresses with aspect ratios varing from 1 to 8 are summarized in Fig. 5. The stress levels increase monotonically with the aspect ratios, which is in agreement with the observations in Fig. 4 (b). The maximum stress in particle with aspect ratio 8 is about 86 MPa. Compared with the aspect

ratio 8 case, the spherical particle has only 58 MPa. Hence, when designing the electrode, the geometrical shape of the particle needs to be taken into account. Especially when taking diffusion induced stress into consideration, the stress levels in ellipsoid particles may differ greatly from the ideal spherical particles.

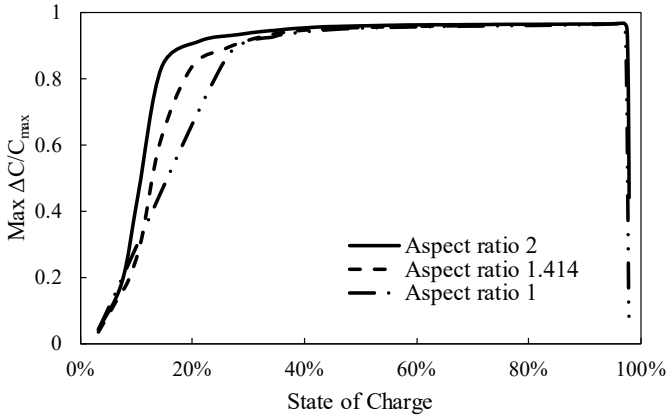

(a)

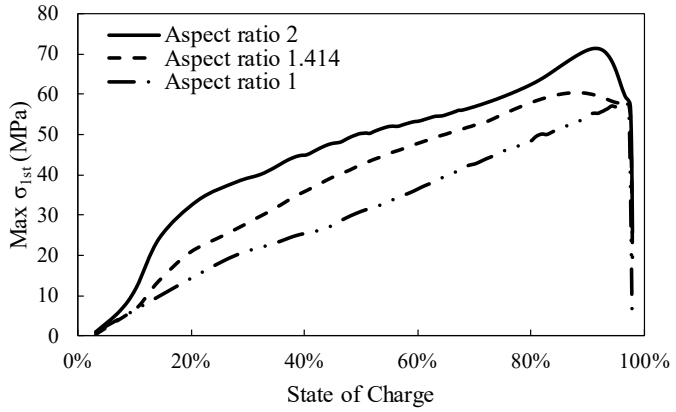

(b)

Fig. 4. (a) Maximum concentration difference and (b) maximum first principal stress for ellipsoid particles with different aspect ratios during discharging process. The equivalent radius of all three cases is 1 μm.

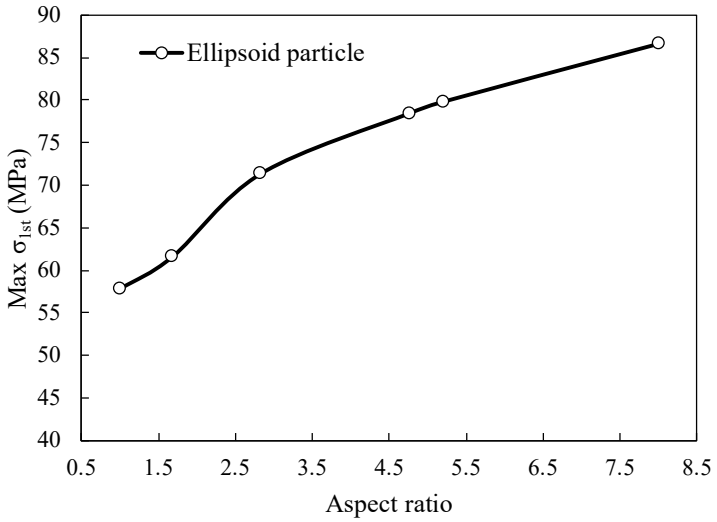

Fig. 5. Maximum first principal stress in ellipsoid particles with different aspect ratios.

The stresses in the realistic particles were also studied compared with the spherical particle. The maximum concentration difference and first principal stress for the spherical and realistic particles with an equavalent radius 0.402 μm are plotted in Fig. 6. The history of maximum concentration difference and first principal stress in Fig. 6 has a similar trend as in Fig. 4. Like elliptical particles, the concentration difference of the realistic particle is much higher than the spherical particle at the initial stage. Comparing Fig. 4(a) with Fig. 6 (a), the concentration differences of the smaller particles at the initial discharging process are smaller than those large particles. This is because small particles have shorter diffusion lengths, leading to less concentration difference. Comparing with maximum first principal stresses, small particles tend to have lower stress.

The morphology of the realistic particle is very different from the spherical ones. Such difference will cause huge differences in diffusion process and stress accumulation. As shown in Fig. 7, for realistic $LiFePO_4$ particles, although the core-shell structure is formed, the concentration distributions are very different from the spherical particle (see Fig. 2 (a)). Besides, the maximum stress of the realistic particle may not necessarily occur in the center.

To quantify the stress levels of the realistic particles, the maximum first principal stresses of spherical and realistic particles with different particle sizes are plotted in Fig. 8. For spherical particles, the stress levels increase with the particle size, which is in good agreement with Zhao's results [22]. The maximum stress in the 1.5-μm spherical particle is 62 MPa, and is about 30% higher than the particle with radius 0.25 μm, which is 49 MPa. For realistic particles with equivalent radius of 0.402 μm and 0.548 μm, the stresses are about 68 MPa and 75 MPa, respectively, which are approximately 30% and 40% higher than the spherical particles with the same equavalent radius.

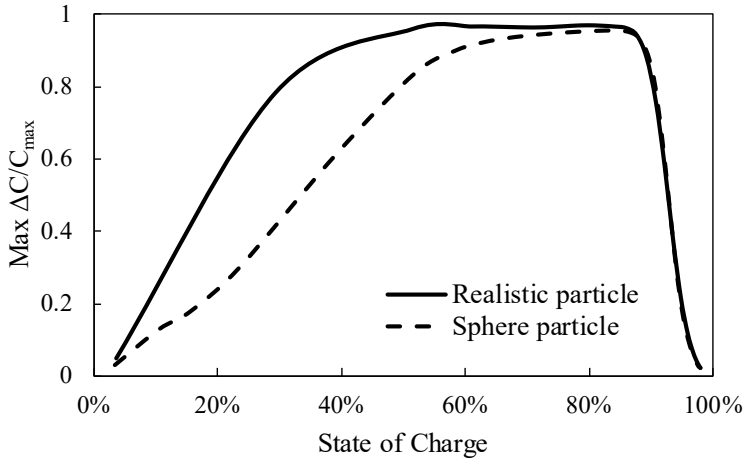

(a)

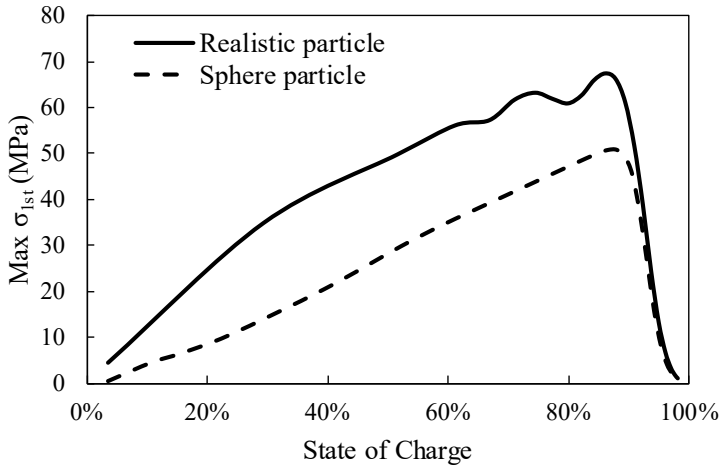

(b)

Fig. 6. Maximum concentration difference and first principal stress for spherical and realistic particles during discharging process. The equivalent radius for both cases are 0.402 μm. (a) Maximum concentration difference; (b) Maximum first principal stress.

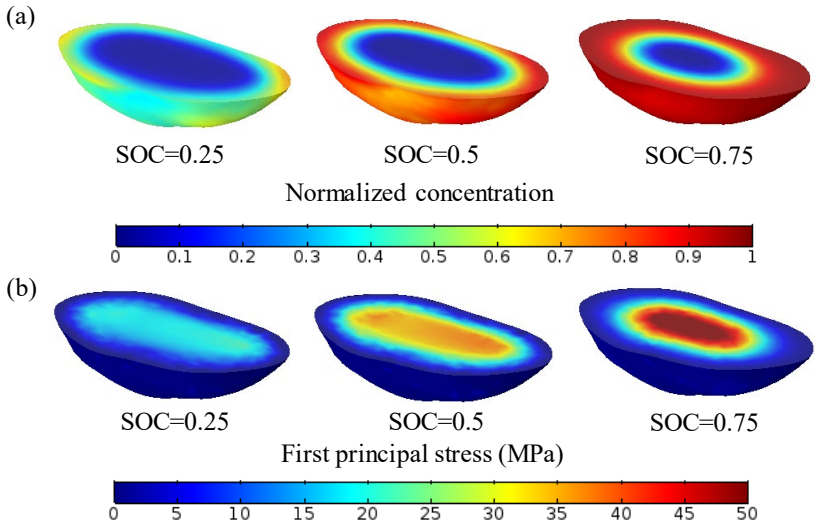

Fig. 7. Lithium ion concentration and hydrostatic stresses for different SOC for realistic $LiFePO_4$ particle with 0.402 μm equivalent radius. (a) Concentration distributions; (b) First principal stresses.

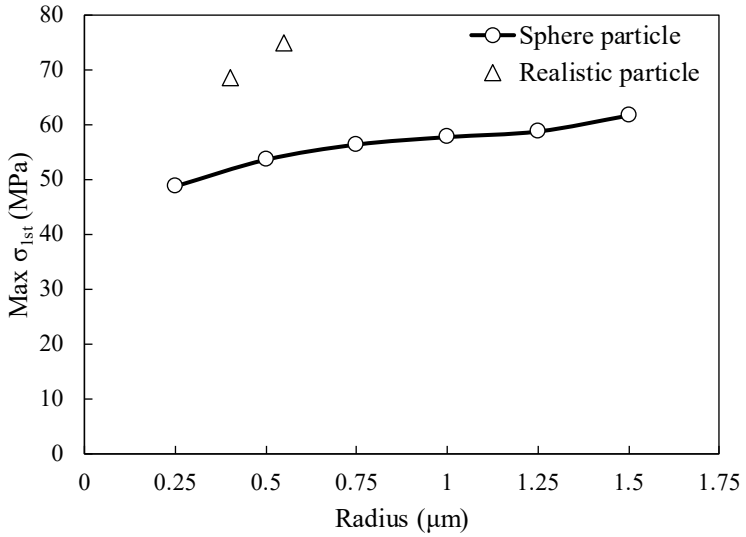

Fig. 8. Maximum first principal stresses of spherical and realistic particles.

5. Conclusions

In this paper, the phase separation and diffusion induced stresses in $LiFePO_4$ particles under potentiostatic discharging process have been simulated using the phase field method. The conclusions are summarized as follows:

(1) The diffusion process in $LiFePO_4$ particles is strongly influenced by particle shapes, especially at the initial lithiation stage. Stresses in the realistic particles are higher than idealized spherical ones. For realistic particles with equivalent radius of 0.402

μm and 0.548 μm, the stresses are about 68 MPa and 75 MPa, respectively, which are approximately 30% and 40% higher than the spherical particles with the same equivalent radius.

(2) The stress levels increase with the increasing aspect ratios in ellipsoid particles. The maximum stress in particle with an aspect ratio 8 is about 86 MPa, while the spherical particle with the same volume has the value of 58 MPa, which is only about 67% of the aspect ratio 8 ellipsoid case.

(3) Stresses increase with particle sizes for spherical particles. The maximum stress in 1.5 μm spherical particle is 62 MPa and is about 30% higher than particle with radius 0.25 μm.

(4) During the discharge, the compressive stresses build up in shell regions and tensile stresses accumulate in the core areas.

(5) The hydrostatic stress has a strong relationship with lithium ion concentration. The hydrostatic stresses and first principal stresses tend to shift from lower values to higher values as the particle takes in more lithium ions.

(6) The diffusion induced stresses are relevant to maximum concentration difference. High concentration difference will cause high stresses.

Acknowledgement

Linmin Wu acknowledges the financial support provided by Purdue Research Foundation doctoral research award. This research used resources of the Advanced Photon Source, a U.S. Department of Energy (DOE) Office of Science User Facility operated for the DOE Office of Science by Argonne National Laboratory under Contract No. DE-AC02-06CH11357. The micro-

tomography data was collected at the X-ray Operations and Research beamlines 32-ID-C and 2-BM at the Advanced Photon Source, Argonne National Laboratory.

List of Figures

List of Tables

References

[1] J. M. Tarascon and M. Armand, "Issues and challenges facing rechargeable lithium batteries," *Nature,* vol. 414, pp. 359-367, 11/15/print 2001.

[2] N. Nitta, F. Wu, J. T. Lee, and G. Yushin, "Li-ion battery materials: present and future," *Materials Today,* vol. 18, pp. 252-264, 2015/06/01/ 2015.

[3] C. Liu, Z. G. Neale, and G. Cao, "Understanding electrochemical potentials of cathode materials in rechargeable batteries," *Materials Today,* vol. 19, pp. 109-123, 2016/03/01/ 2016.

[4] L.-X. Yuan, Z.-H. Wang, W.-X. Zhang, X.-L. Hu, J.-T. Chen, Y.-H. Huang*, et al.*, "Development and challenges of $LiFePO_4$ cathode material for lithium-ion batteries," *Energy & Environmental Science,* vol. 4, pp. 269-284, 2011.

[5] W.-J. Zhang, "Structure and performance of $LiFePO_4$ cathode materials: A review," *Journal of Power Sources,* vol. 196, pp. 2962-2970, 2011/03/15/ 2011.

[6] D. Li and H. Zhou, "Two-phase transition of Li-intercalation compounds in Li-ion batteries," *Materials Today,* vol. 17, pp. 451-463, 2014/11/01/ 2014.

[7] G. Chen, X. Song, and T. J. Richardson, "Electron Microscopy Study of the $LiFePO_4$ to $FePO_4$ Phase Transition," *Electrochemical and Solid-State Letters,* vol. 9, pp. A295-A298, June 1, 2006 2006.

[8] L. Laffont, C. Delacourt, P. Gibot, M. Y. Wu, P. Kooyman, C. Masquelier*, et al.*, "Study of the $LiFePO_4/FePO_4$ Two-Phase System by High-Resolution Electron Energy Loss Spectroscopy," *Chemistry of Materials,* vol. 18, pp. 5520-5529, 2006/11/01 2006.

[9] J. Wang and X. Sun, "Olivine LiFePO4: the remaining challenges for future energy storage," *Energy & Environmental Science,* vol. 8, pp. 1110-1138, 2015.

[10] J. Wang and X. Sun, "Understanding and recent development of carbon coating on $LiFePO_4$ cathode materials for lithium-ion batteries," *Energy & Environmental Science,* vol. 5, pp. 5163-5185, 2012.

[11] H. C. Shin, W. I. Cho, and H. Jang, "Electrochemical properties of the carbon-coated $LiFePO_4$ as a cathode material for lithium-ion secondary batteries," *Journal of Power Sources,* vol. 159, pp. 1383-1388, 2006/09/22/ 2006.

[12] M. Safari and C. Delacourt, "Aging of a Commercial Graphite/$LiFePO_4$ Cell," *Journal of The Electrochemical Society,* vol. 158, pp. A1123-A1135, October 1, 2011 2011.

[13] Y. Zhang, C.-Y. Wang, and X. Tang, "Cycling degradation of an automotive $LiFePO_4$ lithium-ion battery," *Journal of Power Sources,* vol. 196, pp. 1513-1520, 2011/02/01/ 2011.

[14] C. M. Julien, A. Mauger, and K. Zaghib, "Surface effects on electrochemical properties of nano-sized $LiFePO_4$," *Journal of Materials Chemistry,* vol. 21, pp. 9955-9968, 2011.

[15] L. Castro, R. Dedryvère, J.-B. Ledeuil, J. Bréger, C. Tessier, and D. Gonbeau, "Aging Mechanisms of $LiFePO_4$/Graphite Cells Studied by XPS: Redox Reaction and Electrode/Electrolyte Interfaces," *Journal of The Electrochemical Society,* vol. 159, pp. A357-A363, January 1, 2012 2012.

[16] L. Wu, Y. Wen, and J. Zhang, "Three-Dimensional Finite Element Study on Li Diffusion Induced Stress in FIB-SEM Reconstructed LiCoO2 Half Cell," *Electrochimica Acta,* 2016.

[17] L. Wu, X. Xiao, Y. Wen, and J. Zhang, "Three-dimensional finite element study on stress generation in synchrotron X-ray tomography reconstructed nickel-manganese-cobalt based half cell," *Journal of Power Sources,* vol. 336, pp. 8–18, 2016.
[18] L. Wu, Y. Zhang, Y.-G. Jung, and J. Zhang, "Three-dimensional phase field based finite element study on Li intercalation-induced stress in polycrystalline LiCoO2," *Journal of Power Sources,* vol. 299, pp. 57-65, 12/20/ 2015.
[19] J. Park, W. Lu, and A. M. Sastry, "Numerical Simulation of Stress Evolution in Lithium Manganese Dioxide Particles due to Coupled Phase Transition and Intercalation," *Journal of The Electrochemical Society,* vol. 158, pp. A201-A206, 2011.
[20] S. Renganathan, G. Sikha, S. Santhanagopalan, and R. E. White, "Theoretical Analysis of Stresses in a Lithium Ion Cell," *Journal of The Electrochemical Society,* vol. 157, pp. A155-A163, 2010.
[21] L. Wu, X. Xiao, Y. Wen, and J. Zhang, "Three-dimensional finite element study on stress generation in synchrotron X-ray tomography reconstructed nickel-manganese-cobalt based half cell," *Journal of Power Sources,* vol. 336, pp. 8-18, 2016/12/30/ 2016.
[22] K. Zhao, M. Pharr, J. J. Vlassak, and Z. Suo, "Fracture of electrodes in lithium-ion batteries caused by fast charging," *Journal of Applied Physics,* vol. 108, p. 073517, 2010.
[23] Y.-T. Cheng and M. W. Verbrugge, "Evolution of stress within a spherical insertion electrode particle under potentiostatic and galvanostatic operation," *Journal of Power Sources,* vol. 190, pp. 453-460, 2009.
[24] X. Zhang, A. M. Sastry, and W. Shyy, "Intercalation-Induced Stress and Heat Generation within Single Lithium-Ion Battery Cathode Particles," *Journal of The Electrochemical Society,* vol. 155, pp. A542-A552, 2008.
[25] X. Zhang, W. Shyy, and A. Marie Sastry, "Numerical Simulation of Intercalation-Induced Stress in Li-Ion Battery Electrode Particles," *Journal of The Electrochemical Society,* vol. 154, pp. A910-A916, 2007.
[26] L. Wu and J. Zhang, "Ab initio study of anisotropic mechanical properties of LiCoO2 during lithium intercalation and deintercalation process," *Journal of Applied Physics,* vol. 118, p. 225101, 2015.
[27] Y.-T. Cheng and M. W. Verbrugge, "The influence of surface mechanics on diffusion induced stresses within spherical nanoparticles," *Journal of Applied Physics,* vol. 104, p. 083521, 2008/10/15 2008.
[28] Y.-T. Cheng and M. W. Verbrugge, "Diffusion-Induced Stress, Interfacial Charge Transfer, and Criteria for Avoiding Crack Initiation of Electrode Particles," *Journal of The Electrochemical Society,* vol. 157, pp. A508-A516, April 1, 2010 2010.
[29] K. Zhao, M. Pharr, J. J. Vlassak, and Z. Suo, "Inelastic hosts as electrodes for high-capacity lithium-ion batteries," *Journal of Applied Physics,* vol. 109, p. 016110, 2011/01/01 2011.
[30] W. H. Woodford, Y.-M. Chiang, and W. C. Carter, "“Electrochemical Shock” of Intercalation Electrodes: A Fracture Mechanics Analysis," *Journal of The Electrochemical Society,* vol. 157, pp. A1052-A1059, October 1, 2010 2010.
[31] J. Hun, M. Chung, M. Park, S. Woo, X. Zhang, and A. Marie, "Generation of Realistic Particle Structures and Simulations of Internal Stress: A Numerical/AFM Study of $LiMn_2O_4$ Particles," *Journal of The Electrochemical Society,* vol. 158, pp. A434-A442, April 1, 2011 2011.

[32] W. Wu, X. Xiao, M. Wang, and X. Huang, "A Microstructural Resolved Model for the Stress Analysis of Lithium-Ion Batteries," *Journal of The Electrochemical Society,* vol. 161, pp. A803-A813, 2014.
[33] C.-K. ChiuHuang and H.-Y. Shadow Huang, "Stress Evolution on the Phase Boundary in $LiFePO_4$ Particles," *Journal of The Electrochemical Society,* vol. 160, pp. A2184-A2188, January 1, 2013 2013.
[34] L.-Q. Chen, "Phase-Field Models for Microstructure Evolution," *Annual Review of Materials Research,* vol. 32, pp. 113-140, 2002.
[35] L. Chen, H. W. Zhang, L. Y. Liang, Z. Liu, Y. Qi, P. Lu*, et al.*, "Modulation of dendritic patterns during electrodeposition: A nonlinear phase-field model," *Journal of Power Sources,* vol. 300, pp. 376-385, 2015/12/30/ 2015.
[36] J. A. Warren, R. Kobayashi, and W. Craig Carter, "Modeling grain boundaries using a phase-field technique," *Journal of Crystal Growth,* vol. 211, pp. 18-20, 2000/04/01/ 2000.
[37] T. T. Nguyen, J. Yvonnet, Q. Z. Zhu, M. Bornert, and C. Chateau, "A phase-field method for computational modeling of interfacial damage interacting with crack propagation in realistic microstructures obtained by microtomography," *Computer Methods in Applied Mechanics and Engineering,* vol. 312, pp. 567-595, 2016/12/01/ 2016.
[38] C. Miehe, H. Dal, L. M. Schänzel, and A. Raina, "A phase-field model for chemo-mechanical induced fracture in lithium-ion battery electrode particles," *International Journal for Numerical Methods in Engineering,* vol. 106, pp. 683-711, 2016.
[39] L. Chen, F. Fan, L. Hong, J. Chen, Y. Z. Ji, S. L. Zhang*, et al.*, "A Phase-Field Model Coupled with Large Elasto-Plastic Deformation: Application to Lithiated Silicon Electrodes," *Journal of The Electrochemical Society,* vol. 161, pp. F3164-F3172, January 1, 2014 2014.
[40] M. J. Welland, D. Karpeyev, D. T. O'Connor, and O. Heinonen, "Miscibility Gap Closure, Interface Morphology, and Phase Microstructure of 3D LixFePO4 Nanoparticles from Surface Wetting and Coherency Strain," *ACS Nano,* vol. 9, pp. 9757-9771, 2015/10/27 2015.
[41] P. Bai, D. A. Cogswell, and M. Z. Bazant, "Suppression of Phase Separation in $LiFePO_4$ Nanoparticles During Battery Discharge," *Nano Letters,* vol. 11, pp. 4890-4896, 2011/11/09 2011.
[42] D. A. Cogswell and M. Z. Bazant, "Theory of Coherent Nucleation in Phase-Separating Nanoparticles," *Nano Letters,* vol. 13, pp. 3036-3041, 2013/07/10 2013.
[43] Y. Zhao, B.-X. Xu, P. Stein, and D. Gross, "Phase-field study of electrochemical reactions at exterior and interior interfaces in Li-ion battery electrode particles," *Computer Methods in Applied Mechanics and Engineering,* vol. 312, pp. 428-446, 2016/12/01/ 2016.
[44] S. Dargaville and T. W. Farrell, "The persistence of phase-separation in $LiFePO_4$ with two-dimensional Li^+ transport: The Cahn–Hilliard-reaction equation and the role of defects," *Electrochimica Acta,* vol. 94, pp. 143-158, 2013/04/01/ 2013.
[45] M. Z. Bazant, "Theory of Chemical Kinetics and Charge Transfer based on Nonequilibrium Thermodynamics," *Accounts of Chemical Research,* vol. 46, pp. 1144-1160, 2013/05/21 2013.
[46] A. Yamada, H. Koizumi, N. Sonoyama, and R. Kanno, "Phase Change in Li_xFePO_4," *Electrochemical and Solid-State Letters,* vol. 8, pp. A409-A413, August 1, 2005 2005.

[47] T. Maxisch and G. Ceder, "Elastic properties of olivine $LiFePO_4$ from first principles," *Physical Review B,* vol. 73, p. 174112, 05/15/ 2006.
[48] U. S. Kasavajjula, C. Wang, and P. E. Arce, "Discharge Model for $LiFePO_4$ Accounting for the Solid Solution Range," *Journal of The Electrochemical Society,* vol. 155, pp. A866-A874, November 1, 2008 2008.
[49] A. V. Churikov, A. V. Ivanishchev, I. A. Ivanishcheva, V. O. Sycheva, N. R. Khasanova, and E. V. Antipov, "Determination of lithium diffusion coefficient in $LiFePO_4$ electrode by galvanostatic and potentiostatic intermittent titration techniques," *Electrochimica Acta,* vol. 55, pp. 2939-2950, 2010/03/01/ 2010.
[50] J. Lim, Y. Li, D. H. Alsem, H. So, S. C. Lee, P. Bai*, et al.*, "Origin and hysteresis of lithium compositional spatiodynamics within battery primary particles," *Science,* vol. 353, pp. 566-571, 2016.